COMPDYN 2015
5th ECCOMAS Thematic Conference on
Computational Methods in Structural Dynamics and Earthquake Engineering
M. Papadrakakis, V. Papadopoulos, V. Plevris (eds.)
Crete Island, Greece, 25–27 May 2015

CRACKING AND FRACTURE OF HSS BRACES UNDER CYCLIC LOADING

M. Haddad[1], R. Tremblay[2], L. Chen[2], and L. Tirca[3]

[1] United Arab Emirates University
madhar@uaeu.ac.ae

[2] Ecole Polytechnique of Montreal
{robert.tremblay,liang.chen}@polymtl.ca

[3] Concordia University
lucea.tirca@concordia.ca

Keywords: Concentrically Braced Frame, Finite Element Analysis, HSS Brace, Fracture.

Abstract. *Concentric-braced steel frames often fracture at the mid-length of the braces during strong ground motions when the members and connections are properly designed and detailed. The paper describes a finite element model incorporating a damage accumulation model that is able to predict fracture of HSS braces under cyclic loading. Crack initiation is predicted through a refined fracture model. It is shown that the fracture life predicted from finite element analysis based on damage model agrees well with the experimental results and the refined fracture model results. Brace fracture performance is examined for an 8-storey inverted-V concentrically braced frame designed in accordance with the Canadian seismic provisions. Time history analysis of four selected ground motions is carried out on the CBF structure using the OpenSees program. Failure of the braces at the 7th storey is investigated with consideration of the deformation history demand.*

1 INTRODUCTION

Concentrically braced frames (CBFs) frequently use hollow structural steel section (HSS) braces to resist lateral loads and seismic excitations. Fracture of HSS braces was reported after the 1994 Northridge and the 1995 Kobe earthquakes [1]-[2]. Failure of HSS braces has also been observed in braced frame test programs [3]-[6] as shown in Fig. 1. When the end connections are properly designed, fracture typically occurs in the plastic hinge forming at the mid-length of the brace upon global buckling, as a result of high strains developing after local buckling. A review of the fracture life prediction criteria's [7]-[25] revealed that a slightly varied form of the Cyclic Void Growth Model (CVGM) model in [23] for ultra-low cycle fatigue is an appropriate candidate to predict fracture life of steel braces under seismic excitations. With respect to the available plastic hardening models proposed in [26]-[34], it is shown in [35] that the kinematic hardening rule in [27] is a sufficient candidate to model the shift in the yield surface in stress space of HSS brace tests by [36].

Two micromechanics models were presented to simulate ultra-low cycle fatigue of moment connections [23]. The first model is the Degraded Significant Plastic Strain model (DSPS) and the second model is the Cyclic Void Growth Model (CVGM). The two models depend on the cumulative plastic strain, the triaxiality ratio and the characteristic length, to predict fracture. The significant cumulative plastic strain concept is introduced to the DSPS and CVGM models. This concept is compatible with the growth and coalescence mechanisms of the ultra-low cycle fatigue problems. The variation of triaxiality ratio with cycles is not considered in the DSPS model. This variation is taken into account in the CVGM model. Triaxiality is the mean stress over the effective or the Von Mises stress. The triaxiality ratio depends on the load history and the geometry of the specimens (thickness for example). The cyclic fracture life predictions of the CVGM are better than the cyclic results of the DSPS model, especially with variable amplitude loadings. The change in triaxiality is considered with cycling in the latter.

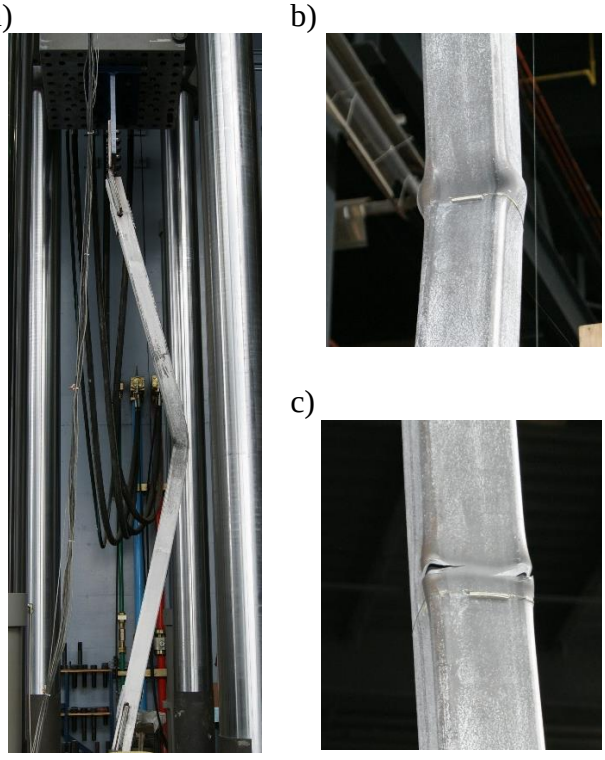

Fig. 1 Quasi-static tests on an HSS127x127x8.0 bracing member [6]: a) Global buckling; b) Local buckling upon brace global buckling; and c) Fracture upon reloading in tension.

Brace fracture prediction represents a critical ingredient for the assessment of the seismic performance of braced steel frames, especially when verifying life safety and collapse prevention limit states. In this paper, a modified finite element model is presented to predict the onset of cracking for HSS specimen 4B of the brace tests in [36]. The significant cumulative plastic strain obtained from the refined CVGM model when cracking first seen is used in a cyclic damage model to predict the fracture life of specimen 4B. The cyclic damage model is needed to simulate the ductile damage initiation when the crack is first seen to failure. The same model is then tested on prediction of the fracture life of a bracing member identical to specimen 4B at the 7th floor level of an 8-storey CBF subjected to seismic ground motion records.

2 FINITE ELEMENT MODEL DESCRIPTION

The combined isotropic kinematic hardening material model was used in the finite element analysis with data type equal to half cycle. This model is capable of simulating the expansion, contraction and the shift of the yield surface in stress space to model the brace behavior under cyclic loading. The shift in the yield surface is a function of the plastic strains and the plastic hardening modulus. The shift (translation) of the yield surface is subtracted from the corresponding stresses according to the kinematic hardening rule in [27], as described in [35]. The engineering stress strain curves obtained from coupon tests on HSS material in [37]-[39] were converted to true stress strain curves that were used here in the finite element model of specimen 4B. The true stress strain curves for walls and corners of specimen 4B in addition to the gusset plates are shown in Fig. 2.

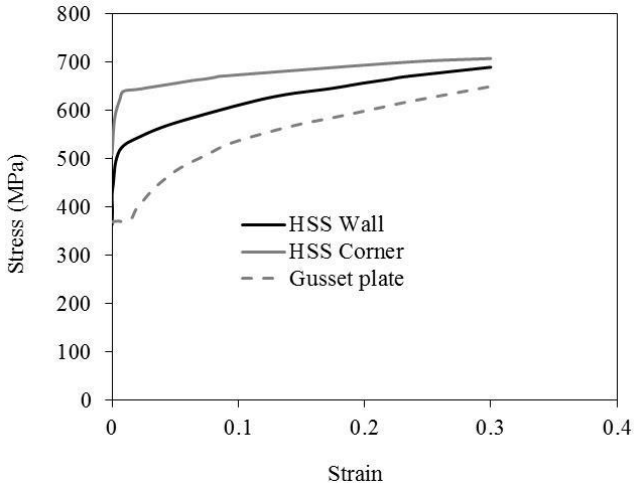

Fig. 2 Stress strain curve

Specimen 4B was designed according to the weak brace strong gusset approach. The tensile capacity of the gusset was greater than the tensile capacity of the brace. Two ways are possible to prevent the net-section fracture. The first way is by using reinforcement plates and the other way is by rounding the fillet weld to close the slot. Both ways are sufficient to prevent net-section fracture. Specimen 4B was tested when rounding the weld even though it is more practical to use reinforcement plates. The detail of the slotted hole at the end of the weld should not affect the brace fracture response since fracture developed at the brace mid-length.

The finite element analysis was performed using the Abaqus code [40]. The use of a four-node quadrilateral shell element (S4R) in modelling steel braces accounts for in-plane and out-of-plane deformations and allows for changes in thickness with deformation. S4R is a re-

duced integration element with three translational and three rotational degrees of freedom per node. Seven integration points were adopted through thickness of the S4R element. A high mesh density was used at the mid-length plastic hinge of the HSS. The element aspect ratio in this region was 1. The gusset plates were connected to the HSS by the nodes on their interfaces. The number of nodes, elements used in modeling specimen 4B, were 16730, 13580, respectively. Fixed brace end conditions were used. It is worth mentioning that using shell elements in modeling braces subjected to cyclic loading is better than using solid elements. The solid elements are not able to simulate the kink at the mid-length of the brace, while this behavior is evident when using shell elements [41]. From experience on modeling concentric braces subjected to cyclic applied displacements, it is more convenient to use multiple integration points through the thickness of one shell element than staking solid elements with one integration point for each solid element. The number of integration points will have an effect on the local behavior and will not have pronounced effect on global behavior. In addition, solid elements are stiffer than shell elements.

The finite element analysis was carried out in two stages. First mode elastic buckling analysis was created in the specimens in the first stage. The initial imperfection to match the measured camber and the cyclic end displacements were then applied in the second stage where nonlinear inelastic analysis was adopted to simulate the hysteresis loops. Large deformations are expected; therefore, the geometric nonlinearity was adopted with the material nonlinearity. The Newton-Raphson method was used to solve the nonlinear equilibrium equations in the stability based approach.

3 VALIDATION OF EXPERIEMNTAL TEST

Specimen 4B, characterized by an HSS 152x152x9.5 mm section with 300x25.4 mm gusset plates at each end of the specimen for end connections, has been selected from the brace tests in [36]. Specimen 4B had the largest cross-section and nearly the longest among the specimens tested. The length of the HSS is 4850 mm. The measured free length of the gusset plates was equal to 32 mm. Thus, the total length of the specimen was equal to 4914 mm. The effective slenderness ratio accounting for end flexural restraint by the gusset plates is 59.7 and the width-to-thickness ratio, $(b\text{-}4t)/t$, is 13.0. The yield strength F_y = 442 MPa and the modulus of elasticity E = 196 GPa of the HSS material were obtained from stub column tests.

The experimental and the finite element's axial hysteresis loops are nearly identical in Fig. 3(a), as well as the lateral hysteresis loops showed in Fig. 3(b). In the experiment and the finite element analysis, the specimen was subjected to four elastic cycles of compression-tension loading. During the compressive side of the fifth cycle, the specimen noticeably buckled into a bow shape. Two plastic hinges formed progressively in the free length of the two gusset plates. The full tension side of the same cycle straightened the specimen. The specimen buckled at lower axial displacements in the sixth compressive cycle than in the fifth. This is mainly attributed to the residual elongation, or camber, and to the plastic hinges which had formed at both ends of the specimens. During the same cycle, the bow shape buckling became larger as shown in Fig. 4(a). The two free length plastic hinges formed completely during the sixth compressive cycle with filet weld cracking noticed in the experiment at both the compression and tension sides of the gusset plate adjacent to free length. The weld was not modeled in the finite element model. The compressive loads showed a marked decrease in capacity in the cycles following the fifth cycle. The tension side of the sixth cycle removed the camber and fully yielded the specimen. Stable plastic behavior of the gusset plates was evident at all times during the test and the finite element model.

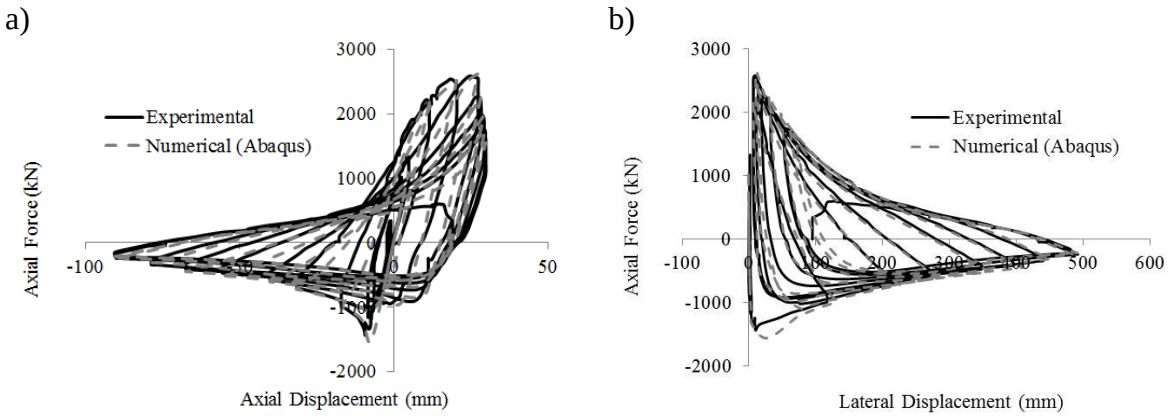

Fig. 3 Hysteresis loops: a) Axial displacement; b) Lateral displacement.

During the compressive side of cycles seven and eight, the specimen shape was changing from a bow shape to a kinked shape, concentrated at the mid-length of the specimen in the experiment and the finite element analysis. This shift in shape indicated the beginning of the development of a plastic hinge at the mid-length of the specimen.

Local buckling at the mid-length plastic hinge began during the compressive side of the ninth cycle, with inward and outward bulging of the specimens' compressive web and flanges, respectively. The outward bulging is closer to the compressive web rather than the tension web. A small inward bow of the tension web was also noticed. The local buckling partially disappeared during the tension side of the same cycle. Local buckling continued to increase in severity during the following cycles. As a result, the buckling shape transformed from a bow shape to a V-shape as shown in Fig. 4(b).

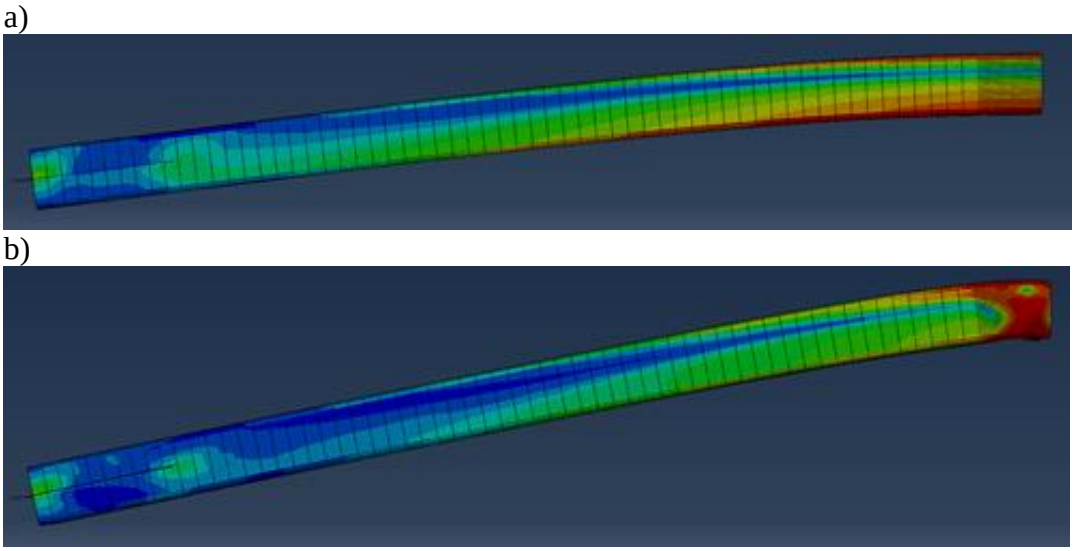

Fig. 4 Lateral buckling: a) Half-bow shape; b) Half-V shape

In the experiment, the continued working of the mid-length region resulted in the tearing of the flanges on the corners at the compressive side of the locally buckled region during the tension excursion of the 11th and final cycle of loading. Small size bent was present at the compressive corners and web at the mid-length plastic hinge upon compressive buckling. This bent is usually severe at the compressive corners (Fig. 5) due to the geometric nature of local buckling and bending. The bent opens during tensile loading and concaves during compres-

sive buckling leading to crack formation due to the cyclic rotational demand and reduction in the cross-sectional area at those locations. Reduction in strain gauge measurements on the compressive side of cycles 11 and 12 is sees in Fig. 6 due to the formation of the small size bent. Tearing and subsequent propagation of the tear resulted in the failure of the specimen upon increasing levels of axial displacement. Failure of the specimen was shifted at a distance of less than the depth of the HSS as shown in Fig. 7.

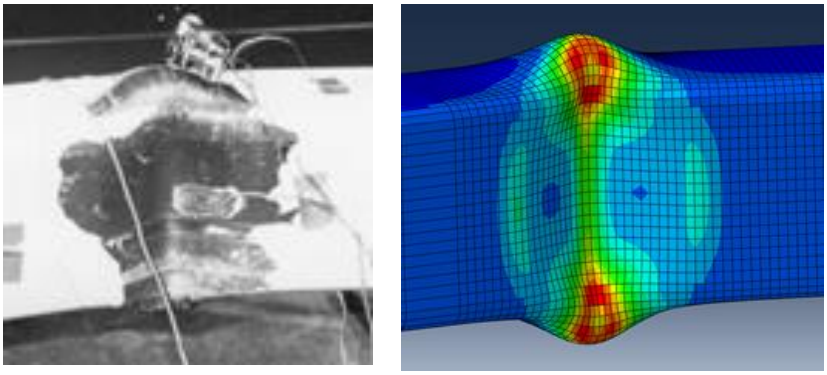

Fig. 5 Small size bent and local buckling

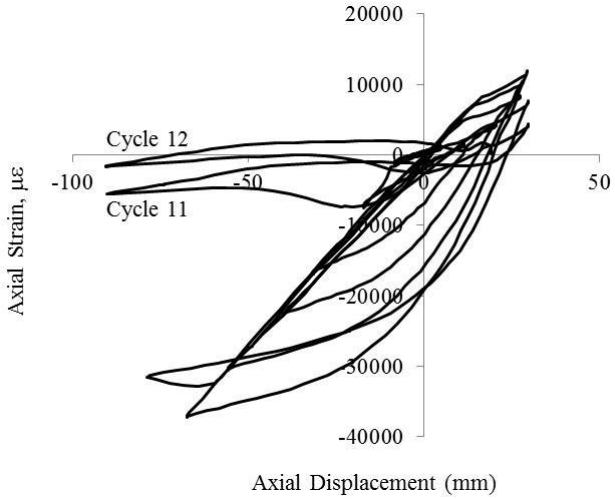

Fig. 6 Axial displacement versus axial strain hysteresis loops

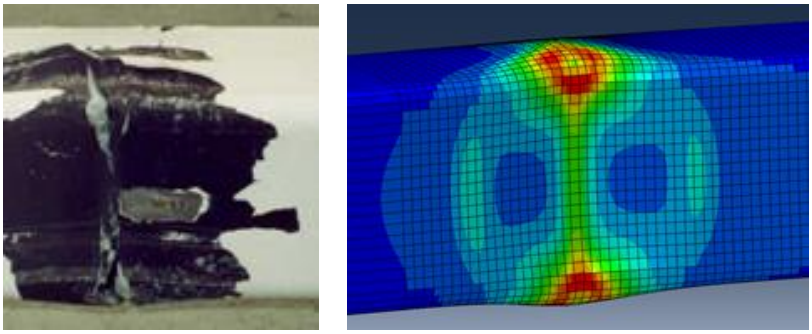

Fig. 7 Fracture of specimen 4B

4 FRACTURE AND DAMAMGE MODELS

During the compressive side of cycles seven and eight, the specimen shape was changing from a bow shape to a kinked shape, concentrated at the mid-length of the specimen in the experiment and the finite element analysis. This shift in shape indicated the beginning of the development of a plastic hinge at the mid-length of the specimen.

An extension to the model proposed in [10] was the CVGM model in [23], which predicts fracture for ultra-low-cycle fatigue (ULCF) braces under cyclic loadings. The CVGM model is based on the following equation (fracture initiates in braces when the degradation in monotonic capacity is less than the cyclic growth in demand):

$$\begin{aligned} &exp(-\lambda_{CVGM}\varepsilon_p)\eta_{monotonic} \leq \\ &\Sigma_{tensile-cycles}\int_{\varepsilon_1}^{\varepsilon_2} exp(|1.5T|)d\varepsilon_t - \\ &\Sigma_{compressive-cycles}\int_{\varepsilon_1}^{\varepsilon_2} exp(|1.5T|)d\varepsilon_c \end{aligned} \tag{1}$$

On the demand side, the equivalent compressive strains are subtracted from the equivalent tensile strains and added incrementally for every cycle of loading taking triaxiality, *T*, into account. Cycles are considered compressive when triaxiality is negative and vice versa.

The capacity side represents the degradation of the monotonic tensile capacity, $\eta_{monotonic}$, due to cyclic loading according to the equation:

$$\eta_{cyclic} = exp(-\lambda_{CVGM}\varepsilon_p)\eta_{monotonic} \tag{2}$$

where:

$$\eta_{monotonic} = \int_0^{\varepsilon_p} exp(1.5T)d\varepsilon_p \tag{3}$$

and ε_p is the cumulative plastic strain.

The monotonic capacity could be obtained from standard coupon or notched bar tests. The monotonic capacity degrades according to the degradation coefficient, λ_{CVGM}. The values of $\eta_{monotonic}$ and λ_{CVGM} were calibrated by conducting notch round bar monotonic and cyclic tests, with two different loading protocols, on seven types of steel made in Japan and the USA [23]. The first loading protocol is to cycle the specimen under constant amplitude high tension and/or low compression cyclic displacements to failure. The second loading protocol is to cycle the specimen under constant predefined low tension and/or compression amplitude displacements, and then to pull the specimen to failure during the last tension cycle. The applied compressive displacements are greater than the applied tensile displacements of specimen 4B (Fig. 3(a)). Strain gauges were deployed at the expected plastic hinge location at the exact mid-length of specimen 4B. The strain gauges were inserted at the neutral axes of the specimen. The strain gauge deployed at the compressive web (Fig. 5) measured the greatest values of strain demand in compression among all strain gauges. Axial strains in compression are greater than axial strains in tension as shown in Fig. 8. Therefore, the significant plastic strains are taken to be compressive minus tensile strains. Plastic strains are accumulated during compressive cycles in the model proposed in [42] where cycles are considered compressive when triaxiality is negative.

For fracture life predictions in the current study, the significant plastic strains are taken to be compressive minus tensile strains on the demand side. Strains are considered compressive when triaxiality is less than -1/3. The -1/3 is a revised simplification for positive maximum principal stress [25]. The maximum principal stress is positive for damage evolution in cyclic loading [18]. For cyclic loading, a slightly modified form of damage evolution by [18] was used in [25]:

$$dD = \begin{cases} (cy)^m d\varepsilon_P & for\, T > -\frac{1}{3}, and \\ 0 & otherwise \end{cases}$$

$$y = \frac{\sigma_{eq}^2}{2E(1-D)^2}\left[\frac{2}{3}(1+\nu)+3(1-2\nu)T^2\right] \tag{4}$$

$$D_c = \int_0^{\varepsilon_P} dD$$

where c and m are material constants, E is the elastic modulus, ν is the Poisson's ratio, σ_{eq} is the effective or the Von Mises stress, dD is damage increment and D_c is the critical damage limit.

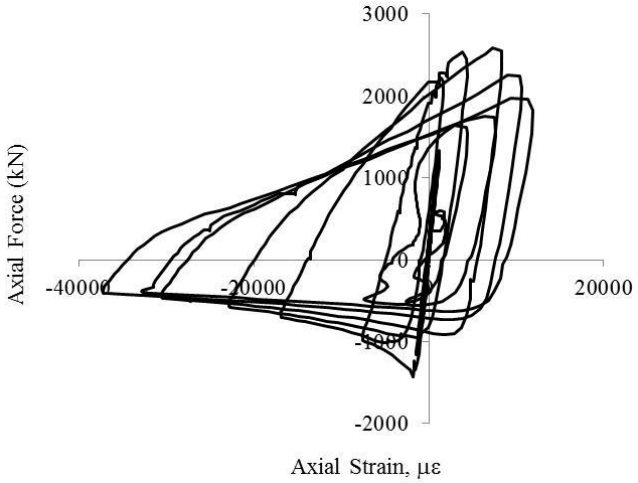

Fig. 8 Axial strain hysteresis loops

For specimen 4B, $\eta_{monotonic}$ is 2.86, which is similar to the value obtained in [23] for AW50 (ASTM A572 Grade 50) steel. In the finite element model, fracture is predicted for specimen 4B during the tensile side of cycle number 12 with λ_{CVGM} equal to 0.11 as shown in Fig. 9. The previous prediction is identical to the fracture of the brace that occurred during the experiment. Using a value of λ_{CVGM} equal to 0.4 or 0.6 for instance results in fracture of the brace during the compressive side of the same cycle (Fig. 9).

The fracture life of specimen 4B is identical to the prediction of the finite element model when considering compressive minus tensile strains. As could be seen from Fig. 9 on the demand side, the critical significant cumulative plastic strain at which tearing or cracking is first seen is 0.67 (tensile side of cycle number 11).

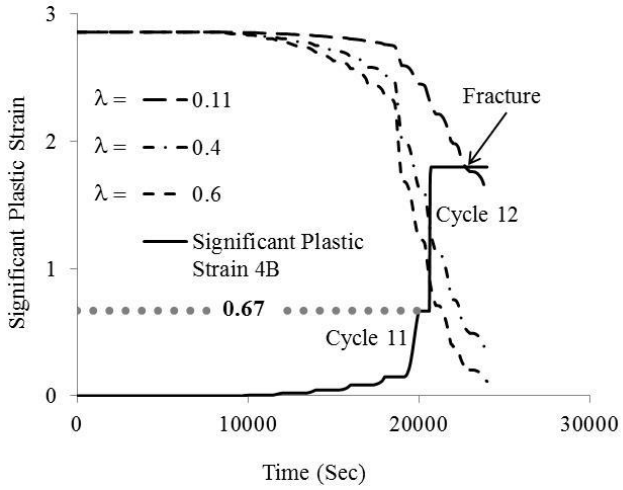

Fig. 9 Fracture life prediction

The cumulative plastic strain is used to specify the location of crack initiation for specimen 4B. The cumulative plastic strain is greater at the external integration point (outer face) than at the internal integration point (inner face) of the element where crack initiates, as shown in Fig. 10. The axial and rotational capacity of the element in consideration is exceeded at the outer faces due to cyclic loading leading to crack initiation at the external face of the element. At these locations, the geometric nature of local buckling leads to early pile up of dislocations that result in formation of slip bands. The continuous cyclic movement along the slip bands or plans leads to the formation of intrusions and extrusions at the outer free surface. At this location, microcracks occur as a result of the formation of slip planes with high shear stress which is often inclined by 45 degrees to the maximum principal stress. Some microcracks join together to form a main crack. When the length of the main crack is sufficient for a stress field to be dominant, the main crack begins to propagate through the brace in the direction normal to the maximum principal stress. The significant plastic strain was equal to 0.67 for the main crack to be dominant for specimen 4B. The main or dominant crack continues to grow until the remaining uncracked cross-section is no longer able to resist the applied load triggering fracture of the brace.

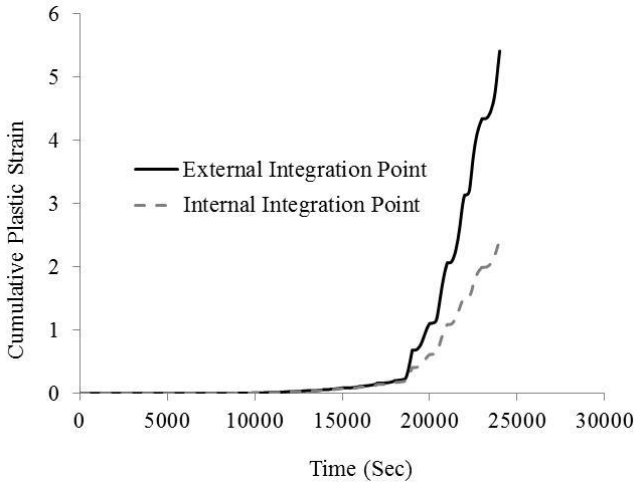

Fig. 10 Cumulative plastic strain at the element where crack initiates

The incremental deformation plasticity theory, based on the significant cumulative plastic strain, was implemented in the damage model to predict the behavior and fracture life of specimen 4B. In the actual test, main crack formed on the compressive side at the mid-length of the specimen where a plastic hinge develops. Hence, the stiffness at this location will gradually decrease causing the specimen to fail. The stiffness in the direction of the maximum principal stress, when the significant cumulative plastic strain reached a value of 0.67, was reduced to zero at the appropriate integration points. The finite element model incorporating the damage model stopped working during the tensile side of the 12th cycle due to numerical error. The axial hysteresis loops of the finite element analysis incorporating the damage model is shown in Fig. 3(a).

5 CASE STUDY

Inverted V-bracing is a popular pattern of brace arrangements for special concentrically braced frames (SCBFs). The brace fracture and fatigue models are used to predict the fracture of braces in a typical 8-storey chevron braced frame located on a site class C in Victoria, British Columbia, subjected to four ground motions. The frame is shown Fig. 11. It is a Type MD (moderately ductile) braced frame designed in accordance with the provisions of NBCC 2010 [43] and CSA S16-09 [44]. The dynamic (response spectrum) analysis method was used to determine seismic design forces in the braces. All braces are square tubing (HSS) conforming to CSA G40.20 with minimum specified F_y = 350 MPa. The braces at the 7th floor level are examined. The size of these braces is HSS 152x152x9.5, which is the same as specimen 4B in [36]. The center line (o/c) length of the brace in the building frame is 5374 mm and the distance between the ductile hinges forming in the gusset plates upon brace buckling is 4836 mm. For specimen 4B, the length between the hinges was 4850 (HSS length) + 32 (two times half the free length) = 4882 mm. The latter is very close to the length of the brace in the prototype building. The same finite element model for specimen 4B is used to examine the fracture life of the brace in the braced frame with a slightly modified version concerning the gusset plate thickness ($t_{Gusset\ plate}$ = 19.1 mm).

Nonlinear seismic response history analyses of the 8-storey structure were carried out using the OpenSees program [45]. The bracing members were modelled using force based nonlinear beam-column elements with fiber discretization of the cross-section [46], [47]. The Giuffré-Menegotto-Pinto (Steel02) material model was selected to account for Bauschinger effect and simulate kinematic-isotropic strain hardening response. The nominal yield strength F_y = 350 MPa was assigned to the steel material. Initial sinusoidal out-of-straightness with maximum amplitude of 1/500 of the unsupported member length was specified for the bracing members. A co-rotational formulation was chosen to consider geometric nonlinearities for the braces. The analyses were performed for four different earthquake records from the PEER ground motion database [48]: Nos. 057, 767, 986, and 1006, as listed in Table I. Hence, a total of eight axial deformation histories were obtained for the two braces, which is of interest because some include several cycles in compression while others have more demand in tension. All records were initially scaled to match the design spectrum.

The time histories axial deformation responses for the two braces (Left and Right) at the 7th floor, as monitored between the two gusset plate plastic hinges in the response history analyses were applied to the finite element model to verify fracture limit states. In the finite element model of the brace, the material properties used for specimen 4B were used after scaling the strength values so that F_y becomes equal to 350 MPa, same as in the response history analyses. The brace axial deformation at yield, δ_y, is 8.3 mm.

In Fig. 12, excellent agreement is found between the brace hysteretic response predicted by the OpenSees and Abaqus models for both braces and all ground motions. In all cases, the braces sustained larger axial deformations in compression as a result of the downward resultant brace load that was imposed at the beam mid-span after buckling of the braces. Yielding in tension only occurred in the Right brace under records Nos. 57, 767, and 1006. Local buckling did not develop in the finite element analysis of the 7th floor braces. These braces did not fracture under the four earthquake records according to the refined fracture and damage models.

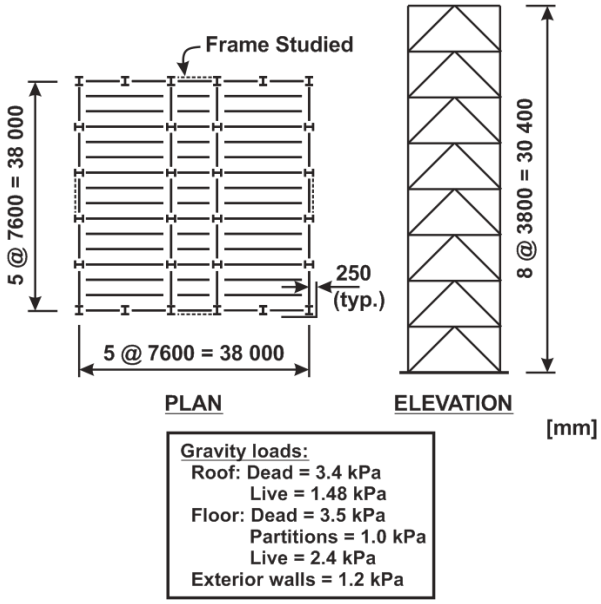

Fig. 11 Prototype building studied

For the ground motion record No. 767, incremental dynamic analysis was carried in OpenSees by applying the following scaling factors, S_F, to the ground motion: 1.5, 2.0 and 2.5. The results for S_F = 1.0, 1.5 and 2.0 are plotted in Fig. 13 for the 4.0-16.0 s time interval. The results are not shown for S_F = 2.5 as inelastic deformations concentrated in braces at another level in the building under that amplified ground motion and the demand on the braces at the 7th floor level reduced. As shown in the figure, the Left brace is subjected to a series of tension excursions before it experiences a series of sequence of significant compression half-cycles. The opposite is observed for the Right brace.

No crack initiation was detected in the Left and Right braces for the previous magnifications of ground motion. For S_F = 2.0, the displacement histories were magnified further by factors of 1.25, 1.5 and 1.75 to detect crack initiation. As could be seen from Fig. 14, crack initiation is detected when magnifying the displacement history by an additional factor between 1.25 and 1.5 for the Left brace while crack initiation is detected when magnifying the displacement history by an additional factor between 1.5 and 1.75 for the Right brace. This particular braced frame therefore possesses significant reserve capacity against fracture of the brace at the 7th floor level. The results also indicate that it is more critical for the brace studied to experience damage when the brace is subjected to a series of tension excursions before compression excursions for the displacement histories used in the case study presented here.

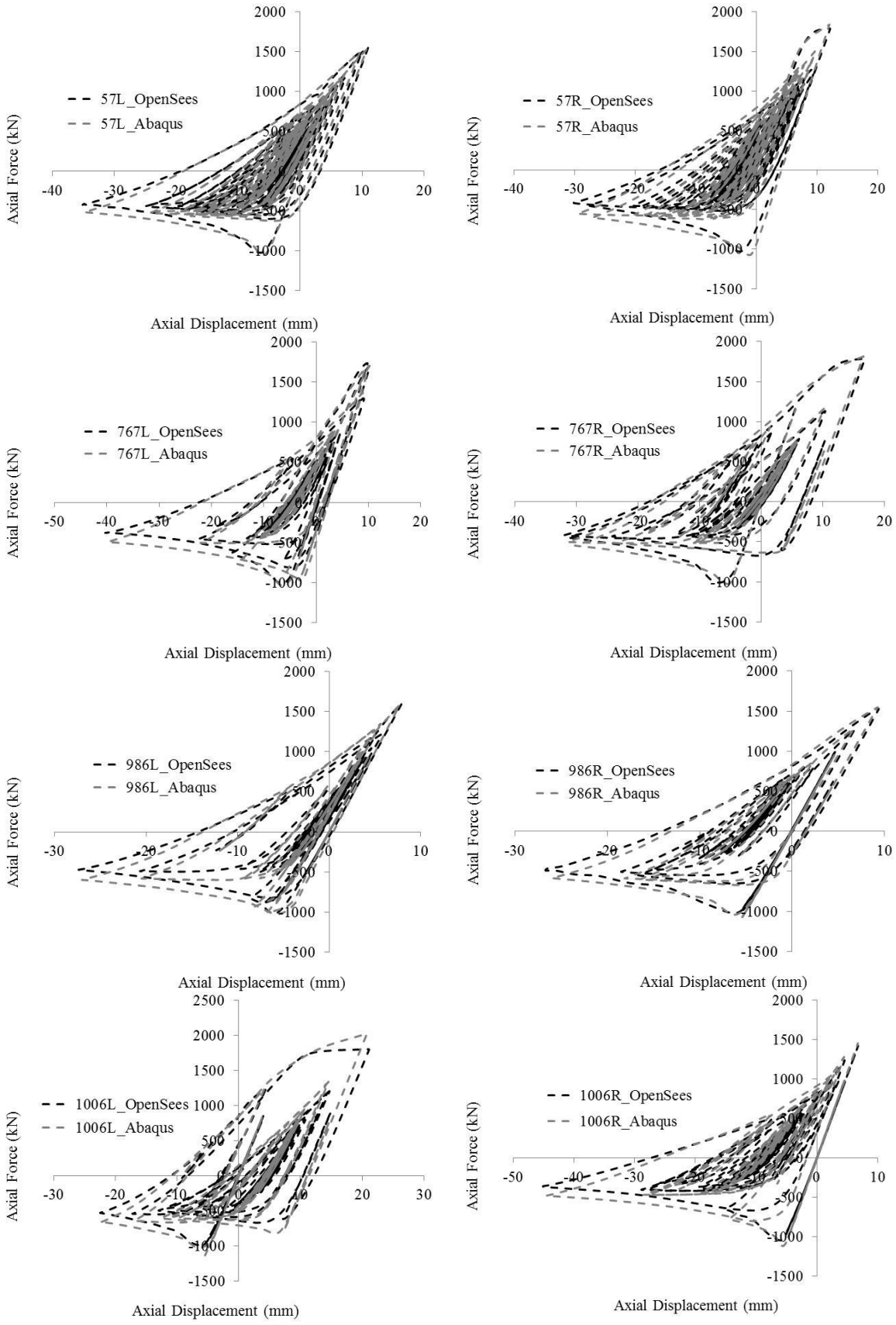

Fig. 12 Axial Hysteresis Loops

No.	Record Sequence Number	Earthquake Name	Station Name	Mag.	Comp.
1	57	1971 San Fernando	Castaic - Old Ridge Route	6.6	291°
2	767	1989 Loma Prieta	Gilroy Array #3	6.9	0°
3	986	1994 Northridge	LA - Brentwood VA Hospital	6.7	195°
4	1006	1994 Northridge	LA - UCLA Grounds	6.7	90°

Table 1: Characteristics of ground motion earthquake records.

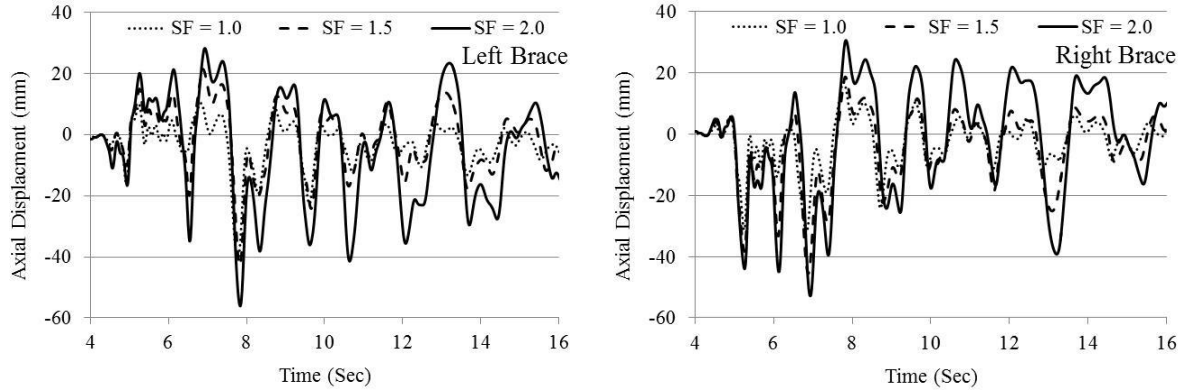

Fig.13 Axial deformation time histories for the Left (L) and Right (R) braces under stepwise incremented ground motion record No. 767.

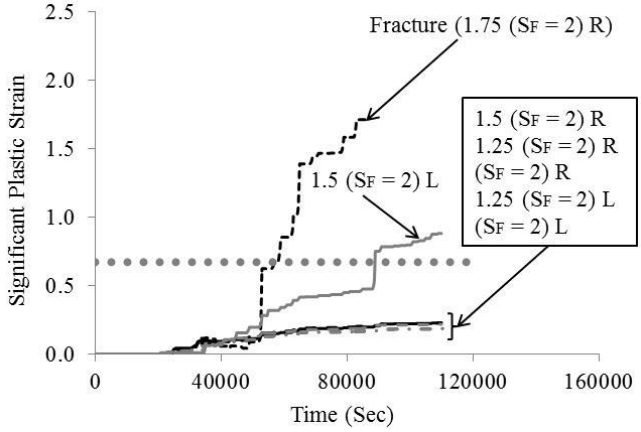

Fig. 14 Significant plastic strain for the Left (L) and Right (R) braces under magnified displacement histories of S_F = 2.0, record No. 767.

6 CONCLUSIONS

Accurate prediction of low-cycle fatigue failure of bracing members is essential for the verification of life safety and collapse prevention limit states when performing seismic assessment of concentrically steel braced frames. A modified finite element model developed in Abaqus was presented to predict the onset of cracking based on the significant cumulative

plastic strain obtained from a refined CVGM model. The model was verified against test data for an HSS specimen. The finite element model could predict the overall cyclic inelastic response of the brace as well as initiation of cracking in the plastic hinge that developed at mid-length of the brace specimen. Nonlinear dynamic analyses were conducted using an OpenSees model in order to obtain time histories of the axial deformation demands imposed to the braces at the 7th floor level of an 8-storey CBF designed in accordance with current Canadian seismic design provisions. The computed time histories of the axial deformation were then applied to the brace finite element model. The analyses showed that fracture of the braces studied would not occur under seismic ground motions corresponding to two times the design earthquake level. Brace fracture was found to be more critical in braces that are subjected to a series of tension excursions before compression excursions are applied.

ACKNOWLEDGMENT

The study was made possible by financial support of the Natural Science and Engineering Council, NSERC Canada and the Individual Research Grant of the UAE University. Many thanks for Brad Shaback, University of Calgary, for providing the experimental data.

APPENDIX

[1] R. Tremblay, M. Bruneau, M. Nakashima, H.G.L. Prion, A. Filiatrault, and R. DeVall, Seismic Design of Steel Buildings: Lessons From the 1995 Hyogoken-Nanbu Earthquake, *Canadian Journal of Civil Engineering*, **23**(3), 727-756, 1996.

[2] R. Tremblay, P. Timler, M. Bruneau, and A. Filiatrault, Performance of Steel Structures During the January 17, 1994 Northridge Earthquake, *Canadian Journal of Civil Engineering*, **22**(2), 138-360, 1995.

[3] X. Tang and S. Goel. Brace Fractures and Analysis of Phase I Structure, *Journal of Structural Engineering*, **115**(8), 1960-1976, 1989.

[4] R. Tremblay, M-H. Archambault, and A. Filiatrault, Seismic Response of Concentrically Braced Steel Frames Made with Rectangular Hollow Bracing Members, *Journal of Structural Engineering*, **129**(12), 1626-1636, 2003.

[5] C.W. Roeder, D.E. Lehman, K. Clark, J. Powell, J.-H. Yoo, K.-C. Tsai, C.-H. Lin, and C.-Y. Wei, Influence of gusset plate connections and braces on the seismic performance of X-braced frames, *Earthquake Engineering and Structural Dynamics*, **40**(XX), 355-374, 2011.

[6] Y. Jiang and R. Tremblay, Influence of PAFs on the inelastic seismic response of steel HSS bracing members, Research Report No. SR14-01, Civil, Geological and Mining Engineering Department, Polytechnique Montreal, Montreal, Canada.

[7] A. M. Freudenthal, The Inelastic Behavior of Engineering Materials and Structures, John Wiley & Sons, New York, 1950.

[8] F. A. McClintock, A. S. Argon, Mechanical Behavior of Materials, Addison-Wesley Publishing Company, 1966.

[9] M. G. Cockcroft, D. J. Latham, Ductility and the Workability of Metals, *Journal of the Institute of Metals*, **96**(2), 33-39, 1968.

[10] J. R. Rice, and D. M. Tracey, On the Ductile Enlargement of Voids in Triaxial Stress Fields, *Journal of the Mechanics and Physics of Solids*, **17**(3), 201-217, 1969.

[11] P. Brozzo, B. Deluka, and R. Rendina, A New Method for the Prediction of Formability in Metal Sheets, *Proceedings of the 7th Biennial Conference on Sheet metal Forming and Formability*, **169**, 41-57, 1972.

[12] L. F. Gillemot, Criterion of Crack Initiation and Spreading, *Engineering Fracture Mechanics*, **8**(1), 239-253, 1976.
[13] D. M. Norris, J. E. Reaugh, B. Moran, and D. F. Quinones, A Plastic-Strain, Mean-Stress Criterion for Ductile Fracture, *Journal of Engineering Materials and Technology*, **100**(3), 279-286, 1978.
[14] M. Oyane, T. K. Sato, Okimoto, and S. Shima, Criteria for Ductile Fracture and Their Applications, *Journal of Mechanical Working Technology*, **4**(l), 65-81, 1980.
[15] A. G. Atkins, Possible Explanation for Unexpected Departures in Hydrostatic Tension-Fracture Strain Relations, *Metal Science*, **15**(2), 81-83, 1981.
[16] V. Tvergaard, Ductile Fracture by Cavity Nucleation between Larger Voids, *Journal of the Mechanics and Physics of Solids*, **30**(4), 265-286, 1982.
[17] V. Tvergaard, and A. Needleman, Analysis of the Cup-Cone Fracture in a Round Tensile Bar, *Acta Metallurgica*, **32**(1), 157-169, 1984.
[18] J. Lemaitre, A course on damage mechanics, Springer-Verlag, 1992.
[19] J. Lemaitre, A continuous damage mechanics model for ductile fracture, *Journal of Engineering Materials and Technology*, **107**(1), 83-89, 1985.
[20] J. Lemaitre, How to use damage mechanics, Nuclear Engineering and Design, **80**(2), 233-245, 1984.
[21] J. Dufailly, and J. Lemaitre, Modeling Very Low Cycle Fatigue, *International Journal of Damage Mechanics*, **4**(2), 153-170, 1995.
[22] P. Matic, G. C. Kirby III, and M. I. Jolles, The Relationship of the Tensile Specimen Size and Geometry Effects to Unique Constitutive Parameters for Ductile Material, NRL Memorandum Report 5936, Mechanics of Materials Branch, Material Science and Technology Division, 1987.
[23] A. M. Kanvinde, and G. G, Deierlein, Micromechanical Simulation of Earthquake-Induced Fracture in Steel Structures, Technical Report 145, John A. Blume Earthquake Engineering Center, Stanford University, California, USA, 2004.
[24] A. M. Kanvinde, and G. G. Deierlein, Cyclic Void Growth Model to Assess Ductile Fracture Initiation in Structural Steels due to Ultra Low Cycle Fatigue, *Journal of Engineering Mechanics*, **133**(6), 701-712, 2007.
[25] Y. L. Huang, and S. A. Mahin, Evaluation of Steel Structure Deterioration with Cyclic Damaged Plasticity, *The 14th World Conference on Earthquake Engineering, Beijing*, China, 2008.
[26] W. Prager, and R. I. Providence, A New Method of Analyzing Stresses and Strains in Work-Hardening Plastic Solids, *ASME Journal of Applied Mechanics*, **23**, 493-496, 1956.
[27] H. Ziegler, A Modification of Prager's Hardening Rule, *Quarterly of Applied Mathematics*, **17**, pp. 55-65, 1959.
[28] Z. Mroz, On the Description of Anisotropic Workhardening, *Journal of the Mechanics and Physics of Solids*, **15**, 163-175, 1967.
[29] Y. F. Dafalias, and E. P. Popov, A Model of Nonlinearly Hardening Materials for Complex Loading, *Acta Mechanica*, **21**, 173-192, 1975.
[30] Y. F. Dafalias, and E. P. Popov, Plastic Internal Variables Formalism of Cyclic Plasticity, *Journal of Applied Mechanics*, **43**, 645-651, 1976.
[31] N. T. Tseng, and G. C. Lee, Simple Plasticity Model of Two-Surface Type, *Journal of Engineering Mechanics*, **109**(3), 795-810, 1983.
[32] P. J. Armstrong, and C. O. Frederick, A Mathematical Representation of the Multiaxial Bauschinger Effect, CEGB Report, RD/B/N/731, Berkeley Nuclear Laboratories, R&D Department, California, USA, 1966.

[33] J. L. Chaboche, Time-Independent Constitutive Theories for Cyclic Plasticity, *International Journal of Plasticity*, **2**(2), 149-188, 1986.
[34] A. F. Bower, Cyclic Hardening Properties of Hard-Drawn Copper and Rail Steel, *Journal of the Mechanics and Physics of Solids*, **37**(4), 455-470, 1989.
[35] M. Haddad, Seismic design of concentrically braced steel frames for earthquakes, PhD Dissertation. Department of Civil Engineering, The University of Calgary, Calgary, A.B., Canada, 2004.
[36] B. Shaback, and T. Brown, Behaviour of square hollow structural steel braces with end connections under reversed cyclic axial loading, *Canadian Journal of Civil Engineering*, **30**(4), 745-753, 2003.
[37] R. K. Bubela, An experimental and analytical study of chevron braced frames with vertical slotted connections, MSc Thesis. Department of Civil Engineering, The University of British Colombia, Vancouver, B.C., Canada, 2003.
[38] J. Aguilera, A. Shaat, and A. Fam, Strengthening T-joints of rectangular hollow steel sections against web buckling under brace axial compression using through-wall bolts, *Thin-Walled Structures*, **56**, 71-78, 2012.
[39] R. Moreau, C. A. Roger, R. Tremblay, and J. A. Packer, Finite element evaluation of the "modified-hidden-gap" HSS slotted tube-to-plate connection, *Connections VII, 7th International Workshop on Connections in Steel Structures*, Timisoara, Romania. 30 May - 2 June, 2012, 10p.
[40] Abaqus, 2011. User's Manual, Version, 11.6, Hibbitt, Karlsson, and Sorensen, Inc., Providence, RI.
[41] S. Santagati, D. Bolognini, and R. Nascimbene, Strain Life Analysis at Low-Cycle Fatigue on Concentrically Braced Steel Structures with RHS Shape Braces, *Journal of Earthquake Engineering*, **16**(S1), 2012, 107-137. doi:10.1080/13632469.2012.675840
[42] A. T. Myers, G. G. Deierlein, and A. M. Kanvinde, Testing and probabilistic simulation of ductile fracture initiation in structural steel components and weldments, Report No. 170. Department of Civil and Environmental Engineering, Stanford University, San Francisco, California, 2009.
[43] NRCC. National Building Code of Canada 2010, 13th ed., National Research Council of Canada, Ottawa, ON, 2010.
[44] CSA. CSA-S16-09, Design of Steel Structures, Canadian Standards Association, Mississauga, ON, 2009
[45] F. McKenna, and G. L. Fenves, Open System for Earthquake Engineering Simulation (OpenSees), Pacific Earthquake Engineering Research Center (PEER), University of California, Berkeley, C.A., 2014. (http://opensees.berkeley.edu/)
[46] A. Aguero, C. Izvernari, and R. Tremblay, Modelling of the Seismic Response of Concentrically Braced Steel Frames using the OpenSees Analysis Environment, *International Journal of Advanced Steel Construction*, **2**(3), 242-274, 2006.
[47] P. Uriz, F. C. Filippou, and S.A. Mahin, Model for Cyclic Inelastic Buckling of Steel Braces, *Journal of Structural Engineering*, **134**(4), 619-628, 2008.
[48] PEER, PEER Strong Ground Motion Database, Pacific Earthquake Engineering Center, 2011. (http://peer.berkeley.edu/nga/)